CHINESE OPTICS LETTERS

Vol. 22, No. 2 | February 2024

Dual-symmetry-perturbed all-dielectric resonant metasurfaces for high-Q perfect light absorption

Junyang Ge (葛俊洋)[1,2], Yixiao Gao (高一骁)[1,2*], Lei Xu (徐 雷)[3], Ning Zhou (周 宁)[4], and Xiang Shen (沈 祥)[1,2,5]

[1] Laboratory of Infrared Materials and Devices, Research Institute of Advanced Technologies, Ningbo University, Ningbo 315211, China

[2] Key Laboratory of Photoelectric Detection Materials and Devices of Zhejiang Province, Ningbo 315211, China

[3] Advanced Optics & Photonics Laboratory, Department of Engineering, School of Science and Technology, Nottingham Trent University, Nottingham NG11 8NS, UK

[4] School of Physics and Optoelectronic Engineering, Hangzhou Institute for Advanced Study, University of Chinese Academy of Sciences, Hangzhou 310024, China

[5] Ningbo Institute of Oceanography, Ningbo 315832, China

*Corresponding author: gaoyixiao@nbu.edu.cn

Received August 5, 2023 | Accepted October 17, 2023 | Posted Online February 27, 2024

We demonstrate a high-Q perfect light absorber based on all-dielectric doubly-resonant metasurface. Leveraging bound states in the continuum (BICs) protected by different symmetries, we manage to independently manipulate the Q factors of the two degenerate quasi-BICs through dual-symmetry perturbations, achieving precise matching of the radiative and nonradiative Q factors for degenerate critical coupling. We achieve a narrowband light absorption with a >600 Q factor and a > 99% absorptance at λ_0 = 1550 nm on an asymmetric germanium metasurface with a 0.2λ_0 thickness. Our work provides a new strategy for engineering multiresonant metasurfaces for narrowband light absorption and nonlinear applications.

Keywords: resonant metasurface; perfect light absorption; bound states in the continuum.
DOI: 10.3788/COL202422.023602

1. Introduction

Photonic bound states in the continuum (BICs) represent a novel category of nonradiative resonant states characterized by infinite Q factors and enhanced electromagnetic near fields. By introducing small perturbations to the structure or modifying the excitation conditions, the radiation channels of a BIC can be opened, leading to the formation of a quasi-BIC state that can interact with free-space radiation. Resonant metasurfaces enabled by BIC attract great research interest due to their ability to achieve high-Q resonance with enhanced light–matter interactions in subwavelength scale and hold promise for a rich variety of applications, including nanolasers[1], nonlinear frequency conversion[2], and sensing[3].

Enhancing light absorption in thin films is critical for various optoelectronic applications. Particularly, high-Q light absorption with a narrowband spectrum, holds significant potential in photodetection[4,5], sensing[6–8], imaging[9], thermal emitters[10], and nonlinear optics[11]. Plasmonic resonances in metal nanostructures are usually exploited to concentrate light into an absorbing medium to increase light absorption. However, their broad linewidth, ohmic heat loss, and low thermal damage threshold limit device performance. Dielectric metasurfaces have emerged as a promising alternative owing to their CMOS-compatible fabrication process and high thermal stability. Resonances in all-dielectric metasurfaces can be used to enhance light confinement and subsequent absorption[12–14]. Critical coupling, achieved when the radiative loss matches the dissipative material loss of dielectrics, enables a maximum absorption of 50% for single-pass transmission. The radiative Q factor tunability of BIC resonances through symmetry perturbations is highly suitable for matching the nonradiative loss rates to realize critical coupling. To further enhance absorption towards unity, a back-reflecting mirror (metal or a distributed Bragg reflector) is utilized under the resonant metasurface to trap the photons within the absorbing layer. However, metal mirrors may introduce additional ohmic loss, and the Bragg reflector would require a complicated fabrication process. Furthermore, such configurations also suffer from broadband reflection outside the absorption band. Alternatively, coherent perfect absorption has been proposed to achieve near-unity absorption, but the required two-sided illumination configuration poses challenges for practical implementation[15].

Degenerate critical coupling offers a promising approach for perfect light absorption[16–18]. This phenomenon requires a pair of resonances that overlap spectrally, with their radiation rates precisely matching the corresponding dissipative loss rates. In

this configuration, each critically coupled resonance contributes 50% absorption. However, meeting such stringent conditions for narrowband absorption is challenging. Tian *et al.* theoretically demonstrated superabsorption in a silicon metasurface by exploiting this concept, where two spectrally overlapped quasi-BIC resonances yielded a maximum absorptance of 84%[19]. Similarly, Yu *et al.* experimentally realized a superabsorbing all-dielectric metasurface with a maximum absorptance of 71% using a similar strategy[20]. Unfortunately, in the aforementioned approaches, both quasi-BIC resonances were protected by the same symmetry [i.e., reflection symmetry (RS)]. Therefore, any structural perturbation would simultaneously alter the radiative Q factors of both resonances. Due to the different field profile of the quasi-BIC resonances, the dissipative loss rate, proportional to $\mathrm{Im}(\varepsilon)|\boldsymbol{E}|^2$, with $\boldsymbol{E}$ representing the electric field of the resonance, varies for different quasi-BIC resonances, and thus it becomes challenging to achieve simultaneous critical coupling for both quasi-BIC resonances, which hinders perfect absorption from being reached.

In this paper, we propose an ultrathin high-Q perfect absorber based on a dual-symmetry perturbed all-dielectric metasurface, which supports degenerate high-Q resonances driven by the physics of BIC. First, we show the characteristics of in-plane electric dipole ($\mathrm{ED_i}$) quasi-BIC resonance protected by RS, and out-of-plane electric dipole ($\mathrm{ED_o}$) quasi-BIC resonance protected by translational symmetry (TS) in the asymmetric dimer metasurface. Next, we investigate the characteristics of Q-factor-mediated absorption enhancement in the resonant germanium (Ge) metasurface. Finally, we discuss the realization of high-Q perfect absorption driven by degenerate critical coupling of quasi-BIC resonances, where perturbations to the TS and RS offer independent tunability of the radiative losses for quasi-BICs to match their respective nonradiative dissipative losses. Our proposed method offers a novel design pathway for narrowband all-dielectric perfect absorbers, which can find applications in emerging optoelectronic devices.

2. Principle and Design

Degenerate critical coupling enables strong optical absorption in thin nanostructures, which employ two spectrally overlapped resonances. According to coupled-mode theory, the absorption in a two-ports system supporting two resonances is given by

$$A=\sum_{i=1,2}\frac{\omega_i^2/(2Q_{Ri}Q_{Ni})}{(\omega-\omega_i)^2+\frac{\omega_i^2}{4}\left(\frac{1}{Q_{Ri}}+\frac{1}{Q_{Ni}}\right)^2}, \tag{1}$$

where ω_i is the resonant radian frequency of the ith resonance; Q_{Ri} and Q_{Ni} are radiative and nonradiative Q factors of the ith resonance. The Q factor characterizing the total energy leakage rate from the resonator is calculated as $1/Q=1/Q_R+1/Q_N$. From Eq. (1), we know that a 100% light absorption could be achieved when the two resonances have the same resonance frequency (i.e., $\omega_1=\omega_2$) and the radiative Q factor matches the nonradiative Q factor for each resonance (i.e., $Q_{R1}=Q_{N1}$, and $Q_{R2}=Q_{N2}$). This condition requires two resonances to be orthogonal to each other so that the resonant frequency can overlap[21]. In addition, the nonradiative loss from material absorption is proportional to $\mathrm{Im}(\varepsilon)|\boldsymbol{E}|^2$, where ε is the complex permittivity of the resonator medium and $\boldsymbol{E}$ is the resonance field profile. However, the field profiles of two resonances at the same frequency usually differ, leading to distinct nonradiative Q factors. Achieving perfect absorption requires that the Q_R of two degenerate resonances be independently controlled to match the corresponding Q_N. An effective solution to this objective lies in investigating quasi-BIC resonances in resonant metasurfaces, where Q factors can be controlled through asymmetry manipulation of a unit cell.

Figure 1 shows the schematic of the proposed all-dielectric high-Q perfect absorber based on a dual-symmetry-perturbed dimer metasurface, which consists of a periodic square array of zigzag-shaped pairs with a period $P=900$ nm, and nanostructures are made of Ge with a thickness $l_z=300$ nm and embedded in silica with a refractive index of 1.45. Ge is a widely utilized material for near-infrared photodetection, and the incorporation of a thin Ge metasurface layer would improve optoelectronic performance[22]. Here, we consider a dispersionless Ge refractive index of $4.275+0.00567i$, exhibiting weak absorption in the telecommunication band[23]. The incident light is polarized along the x axis, with its wave vector perpendicular to the metasurface. The total length along x and the width along y of each cube in the dimer are l_x and l_y, respectively, and half of the dimer spacing is d_1 and the other half is d_2, as depicted in Fig. 1(a). The characteristics of BIC resonances are determined by symmetry. By controlling the values of d_1 and d_2, two types of symmetry can be perturbed. Here, the unit cell is referred to as an unperturbed one when $d_1=d_2=d_0=(P-2l_x)/2$. In this configuration, the corresponding metasurface repeats itself after a translation of $P/2$ along the x-axis, exhibiting TS. When $d_1\neq d_2$, the unit cell loses its RS with respect to the x axis (i.e., the unit cell cannot repeat itself under a σ_x operation). The perturbation of RS could be quantified by $\Delta d=|d_1-d_2|$. When the average distance between d_1 and d_2, denoted as $d_{\mathrm{avg}}=(d_1+d_2)/2$, deviates from d_0, the original TS of the unperturbed metasurface is broken, i.e., the perturbed metasurface can no longer repeat itself when translated along the x axis by a distance of $P/2$, and the strength of TS perturbation is characterized by $\Delta d_{\mathrm{avg}}=|d_{\mathrm{avg}}-d_0|$, as depicted in Figs. 1(b)–1(e).

Figures 2(a) and 2(b) illustrate the two types of BIC resonances in the unperturbed dimer unit cell. Here, the geometric parameters of the unit cell are $l_x=165$ nm and $l_y=330$ nm, and we consider the refractive index of Ge to have a zero imaginary part, neglecting metasurface absorption. The eigenmodes are obtained through a three-dimensional finite-element method-based eigenfrequency solver, and the unit cell has periodic conditions in the x and y directions, and perfectly matched layers are imposed three free-space wavelengths away from the structure in the z direction. Figure 2(a) shows a pair of out-of-plane antiphased electric dipolar resonance, evident from the

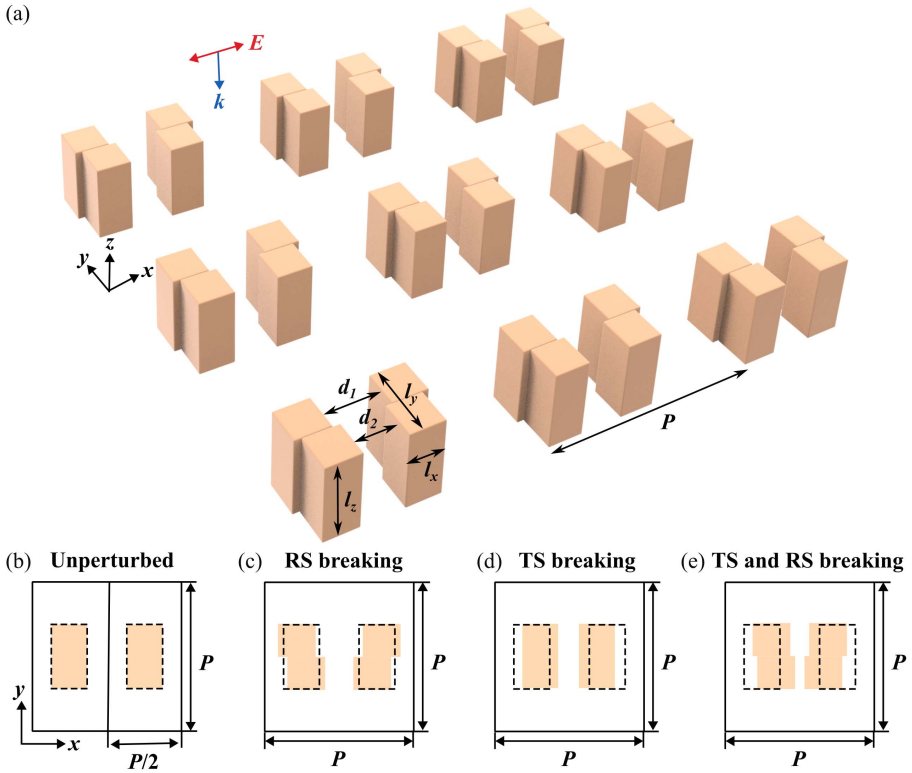

Fig. 1. (a) Schematic for the dimer metasurface. The dimers are arranged in a square lattice with a period of P. The parameters of the dimer unit cell are shown in the lower left corner, where l_x, l_y, and l_z control the size of the dimer, and d_1 and d_2 determine the symmetry properties of the unit cell. (b) Illustration for an unperturbed unit cell with $d_1 = d_2 = d_0 = (P - 2\,l_x)/2$; (c) unit cell with RS breaking characterized by a nonzero $\Delta d = d_1 - d_2$ and $d_{avg} = (d_1 + d_2)/2 = d_0$; (d) unit cell with TS breaking characterized by a nonzero $\Delta d_{avg} = (d_1 + d_2)/2 - d_0$ and $\Delta d = 0$; (e) unit cell with both TS and RS breaking with both nonzero Δd and Δd_{avg}; the dashed frames in (b)–(e) indicate the location of the unperturbed dimer unit cell.

surface charge distribution. Hence, we refer to this resonance as $ED_o - BIC$. While the resonance shown in Fig. 2(b) features a pair of antiphased electric dipolar resonances with their dipole moments aligning in the metasurface plane, which is referred to as $ED_i - BIC$ in subsequent discussions.

Figures 2(c) and 2(d) show the evolution of transmission spectra with varying RS (Δd) and TS (Δd_{avg}) perturbation, when the dimer metasurface is excited by a normally incident plane wave. Through an eigenfrequency calculation, we find $ED_o - BIC$ and $ED_i - BIC$ have resonant wavelengths at 1532.0 and 1572.6 nm, respectively, as denoted by the circles in Figs. 2(c) and 2(d). When only TS perturbation is applied to the dimer metasurface by varying Δd_{avg} from 0 to 120 nm while keeping $\Delta d = 0$, a transmission dip emerges near the $ED_o - BIC$ resonant wavelength at 1532.0 nm when Δd_{avg} becomes nonzero. With Δd_{avg} growing further, the linewidth broadens, accompanied by a blueshift in the resonant wavelength. This behavior indicates the transformation of the nonradiating $ED_o - BIC$ into a quasi-BIC with finite Q-factor that can be accessed by external excitations, as depicted in Fig. 2(c). Throughout the Δd_{avg} tuning process, $ED_i - BIC$ maintains its nonradiating characteristics, showing its robustness to TS perturbation. In contrast, when the dimer metasurface is perturbed solely by RS breaking with $\Delta d_{avg} = 0$ and varying Δd, the $ED_i - BIC$ resonance exhibits a behavior similar to $ED_o - BIC$ when subjected to TS-only perturbation. As Δd increases, a broader linewidth and a blueshifted resonant wavelength are observed. However, it is worth noting that $ED_o - BIC$ cannot be accessed by the plane wave excitation for any value of Δd, indicating that RS perturbation alone cannot cause $ED_o - BIC$ to transition into its radiative quasi-state.

The underlying physics is that the radiation channel of $ED_i - QBIC$ is related to the net dipole moment aligning with the x axis in the perturbed dimer unit cell. We carried out a multipolar expansion of the QBIC resonances in the dimer unit cell using the formulas reported in Ref. [24]. As depicted in Fig. 3(a), $ED_i - BIC$ only has a dominant magnetic dipole (MD) moment m_y, which does not contribute to the out-of-plane radiation. While an ED moment p_x emerges in $ED_i - QBIC$ at $\Delta d =$ 60 nm, which is responsible for the radiation channel opening and interaction with the x-polarized incident plane waves, the amplitude of p_x is proportional to the RS perturbation strength Δd. For the $ED_o - QBICs$, the dimer unit cell consistently possesses an MD moment, regardless of whether the TS perturbation Δd_{avg} is zero or not. The MD moment m_y is synthesized by two adjacent out-of-plane EDs, and two neighboring MDs are antiphased, as indicated by the surface charge distributions in Fig. 3(b). When $\Delta d_{avg} = 0$, neighboring synthetic MDs have

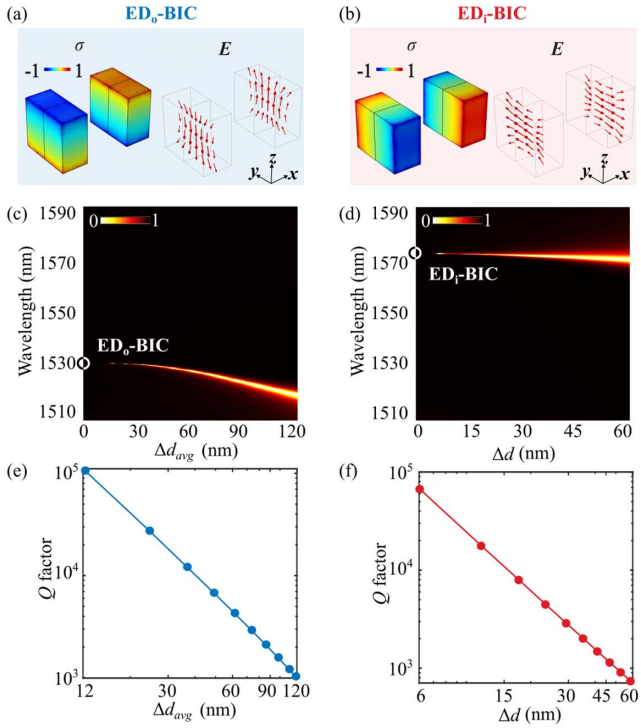

Fig. 2. Surface charge density and vectorial electric field distribution of (a) ED_o − BIC and (b) ED_i − BIC in an unperturbed dimer unit cell. (c) Transmission spectra of a TS-perturbed dimer metasurface as a function of Δd_{avg}; the transmission dip corresponds to ED_o − QBIC, and $\Delta d = 0$. (d) Transmission spectra of an RS-perturbed dimer metasurface as a function of Δd; the transmission dip corresponds to ED_i − QBIC, and $\Delta d_{avg} = 0$. Circles indicate the nonradiative BICs. The Q factors of ED_o − QBIC and ED_i − QBIC against (e) TS-only and (f) RS-only perturbation.

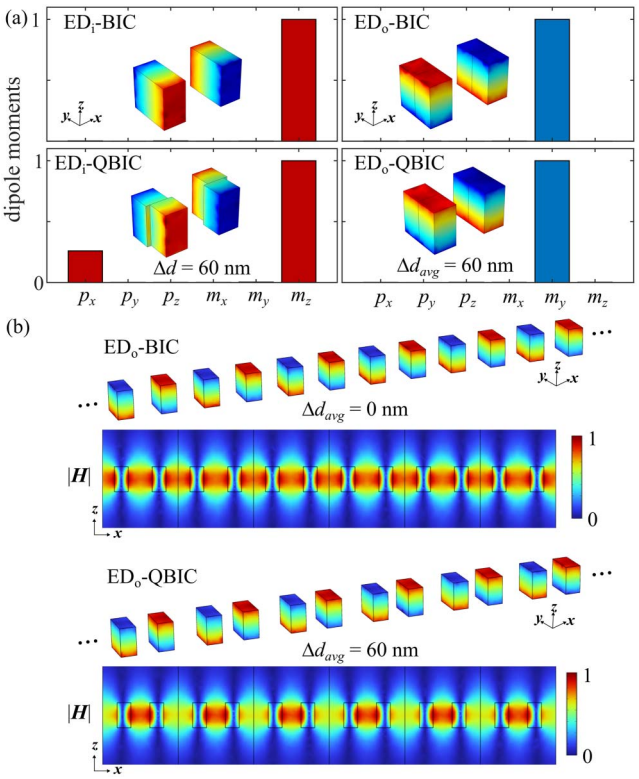

Fig. 3. (a) Normalized dipolar components in ED_o − QBIC and ED_i − QBIC resonances with different Δd_{avg} and Δd perturbations; (b) surface charge distribution and magnetic field of ED_o-QBIC in multipole unit cells of a dimer metasurface with (top) $\Delta d_{avg} = 0$ and (bottom) $\Delta d_{avg} = 60$ nm.

equal amplitudes, as depicted by the magnetic field distribution in Fig. 3(b), leading to the radiation suppression by perfectly destructive interference. However, the introduction of a nonzero Δd_{avg} perturbation leads to neighboring synthetic MD moments being unequal in amplitude, as observed in the magnetic field distribution in Fig. 3(b), thereby breaking the balance of perfectly destructive interference and unlocking the radiation channel[25]. Note that the TS-BIC is closely linked to the recently reported band-folding-induced BICs[26–28]. An eigenfrequency calculation shows that the variation of Q factor against Δd_{avg} and Δd perturbations follows an inverse-square law[29], as depicted in Figs. 2(e) and 2(f), and a diverging Q factor could be confirmed for each resonance when the corresponding symmetry perturbation parameter approaches zero.

This unique feature allows us to independently tune the Q factors of the two QBIC resonances on the same metasurface by perturbing different symmetries. Figure 4(a) shows the transmission spectra under various Δd_{avg} and Δd values when the dimer unit cell experiences a strong TS perturbation ($\Delta d_{avg} = 90$ nm) and a weaker RS perturbation ($\Delta d = 15$ nm). The ED_o − QBIC at 1524.48 nm has a Q factor of 806, while the ED_i − QBIC at 1564.2 nm possesses a higher Q factor of 8845. If the TS perturbation is reduced to $\Delta d_{avg} = 60$ nm while RS perturbation increases to $\Delta d = 30$ nm, both resonances have a similar Q factor, with 1841 for ED_o − QBIC and 2416 for ED_i − QBIC. If we further perturb the dimer metasurface by a lower $\Delta d_{avg} = 30$ nm and a larger $\Delta d = 45$ nm, ED_o − QBIC would have a higher Q factor of 7127 compared to ED_i − QBIC, which has a Q factor of 1141. To further characterize the independent Q factor tuning behavior through dual-symmetry perturbations, we calculated the variations of the Q factor of ED_o − QBIC and ED_i − QBIC in the dual-symmetry perturbation space ($\Delta d_{avg} - \Delta d$), as depicted in Figs. 4(b) and 4(c). It can be observed that the Q factor of ED_o − QBIC is primarily dependent on the strength of TS perturbation (Δd_{avg}), while the Q factor of ED_i − QBIC is determined by the RS perturbation. This observation is consistent with our previous discussion.

Figure 5 shows the Q-factor-mediated resonance-enhanced absorption in the dimer metasurface when considering the extinction coefficient of Ge. The absorptance (A) is calculated by $A = 1 - T - R$, where T and R represent transmittance and reflectance of the normally incident plane wave.

Figures 5(a) and 5(b) show the absorptance spectra as a function of perturbation strength Δd_{avg} and Δd. Here, the resonant wavelength for ED_o − BIC (ED_i − BIC) is 1554 nm (1556 nm) with $l_x = 168$ nm and $l_y = 309.75$ nm. We observe an enhanced absorptance at the resonant wavelength for both QBIC resonances. For ED_o − QBIC, the maximum absorptance of 50% is

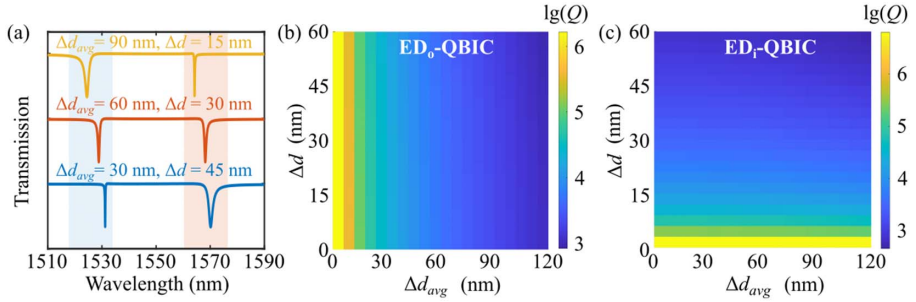

Fig. 4. (a) Transmission spectrum of a dimer lattice with different TS and RS perturbation strengths characterized by Δd and Δd_{avg}; Q factors of (b) ED_o – QBIC and (c) ED_i – QBIC as a function of Δd and Δd_{avg}.

achieved at the wavelength of 1549.6 nm, with a TS-only perturbation of $\Delta d_{avg} = 72.1$ nm, as depicted in Fig. 5(c). For ED_i – QBIC, the absorptance reaches 50% at the wavelength of 1554.6 nm when the RS-only perturbation is $\Delta d = 33$ nm, as depicted in Fig. 5(d). Any other perturbation strength would lead to undercoupling or overcoupling scenarios with an absorptance less than 50%. We further evaluate the radiative and nonradiative Q factors of ED_o – QBIC and ED_i – QBIC through an eigenfrequency calculation. The radiative quality factors Q_R of QBICs are calculated by setting extinction coefficient k to 0, while the nonradiative quality factors could be evaluated by $Q_N = QQ_R/(Q_R - Q)$, with Q representing the overall quality factor that takes into account material absorption. Figures 5(e) and 5(f) display the variation of Q_N and Q_R as a function of the perturbation strength (i.e., Δd_{avg} for ED_o – QBIC and Δd for ED_i – QBIC). Q_R of both QBICs decrease with stronger perturbation, while Q_N values remain nearly the same. The crossing between Q_N and Q_R indicates a critical coupling condition is met, leading to a 50% absorptance[16]. This trend is in agreement with the absorption spectra presented in Figs. 5(a) and 5(b).

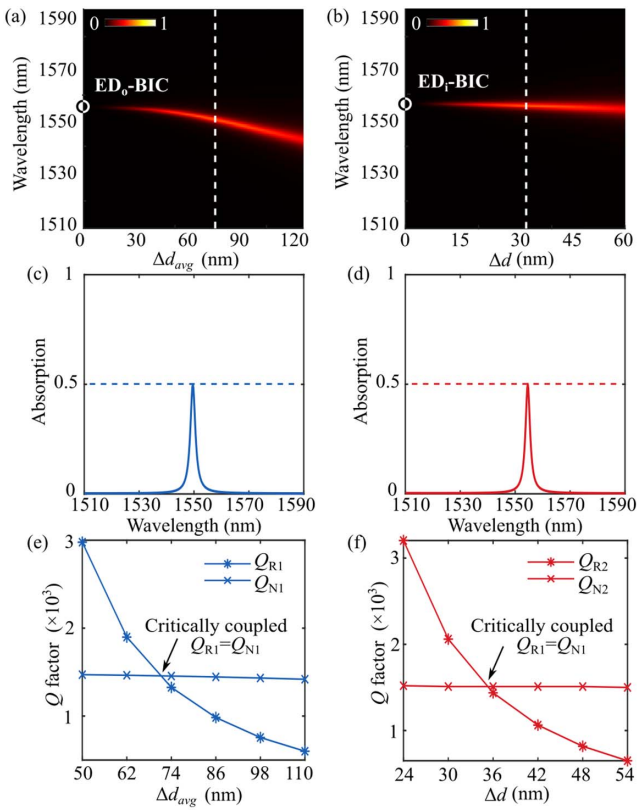

Fig. 5. (a) Absorption spectrum: ED_o – BIC against TS-only perturbation with $\Delta d = 0$; the dashed line indicates that the absorption reaches 50%, corresponding to $\Delta d_{avg} = 72.1$ nm. (b) Absorption spectrum: ED_i – BIC against RS-only perturbation, $\Delta d_{avg} = 0$; the dashed line indicates that the absorption reaches 50%, corresponding to $\Delta d = 33$ nm. Circles indicate the formation of BICs. (c) corresponds to the dashed line in (a), and (d) corresponds to the dashed line in (b). Radiative Q-factor Q_R and nonradiative Q-factor Q_N of (e) ED_o – BIC and (f) ED_i – BIC. The arrows represent the critical coupling points, corresponding to the perturbations $\Delta d_{avg} = 73$ nm and $\Delta d = 35$ nm, respectively.

To achieve degenerate critical coupling, it is necessary for two resonances to not only have matched Q factors, but also the same resonant wavelength. Figure 6 shows the resonant wavelength λ_{res} behavior of ED_o – BIC and ED_i – BIC in an unperturbed dimer metasurface, considering the variation of l_y and l_z. In Fig. 6(a), we vary l_y while keeping $l_x = 165$ nm and $l_z = 300$ nm. The λ_{res} of both BICs exhibit a linear relationship with l_y, but the resonant wavelength of ED_i – BIC changes faster than that of ED_o – BIC as l_y increases. This behavior can be attributed to the modal field of ED_i – BIC oscillating along the y direction, as shown in Fig. 2(b). Similarly, Fig. 6(b) shows that ED_o – BIC is more sensitive to changes in l_z, given its modal field oscillating along the z direction. Here, we keep $l_x = 165$ nm and

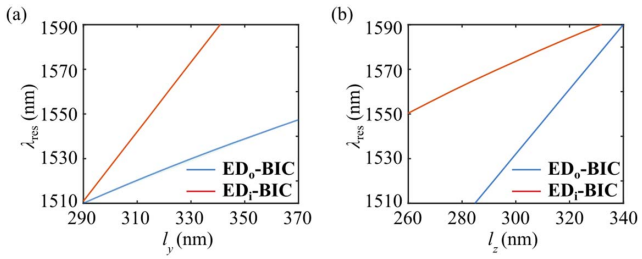

Fig. 6. Resonant wavelengths of ED_o – BIC and ED_i – BIC as a function of (a) l_y and (b) l_z.

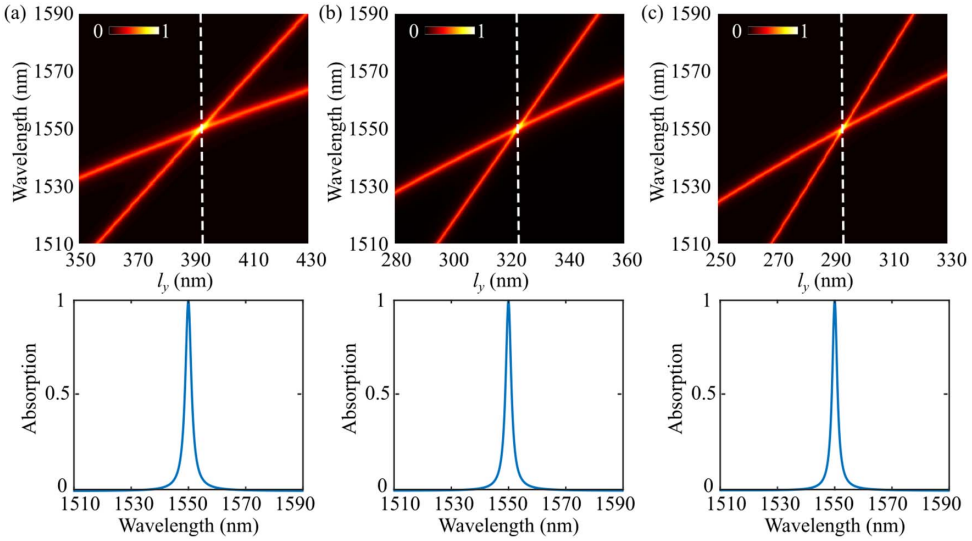

Fig. 7. Absorption spectra of the asymmetric dimer metasurface with (a) $l_x = 100$ nm; (b) $l_x = 150$ nm; and (c) $l_x = 200$ nm, with the resonance crossing triggered by tuning l_y. The white dashed line indicates near-unity absorption occurs, and the lower panels show the corresponding absorption spectra.

$l_y = 330$ nm. By leveraging the different sensitivity behaviors of $\mathrm{ED_o} - \mathrm{BIC}$ and $\mathrm{ED_i} - \mathrm{BIC}$, we can flexibly match the resonant wavelengths of these two types of QBIC resonances by tuning l_y and l_z accordingly.

3. High-*Q* Perfect Absorption

With the knowledge of independent Q factor and resonant wavelengths control of $\mathrm{ED_i} - \mathrm{QBICs}$ and $\mathrm{ED_o} - \mathrm{QBICs}$ in the asymmetric dimer metasurface, perfect absorption enabled by the degenerate critical coupling could be realized at any given wavelength by finely tuning the RS and TS perturbation strength as well as the dimer size. Figure 7(a) shows the absorption spectra of a finely tuned asymmetric dimer metasurface as a function of l_y. Here we set $l_x = 100$ nm, $l_z = 400$ nm, $\Delta d_{\mathrm{avg}} = 160$ nm, and $\Delta d = 46$ nm. The enhanced absorption peaks (~50%) associated with $\mathrm{ED_i} - \mathrm{QBIC}$ and $\mathrm{ED_o} - \mathrm{QBIC}$ intersect at $l_y = 392.56$ nm, where the resonant wavelength locates at 1550 nm. The absorption spectrum at $l_y = 392.56$ nm is plotted in the lower panel of Fig. 7(a), exhibits an absorptance of 99.90% at 1550 nm, surpassing the results reported in Ref. [19], and the Q factor of absorption peak is 613. Furthermore, by using a thicker dimer with a larger l_x (e.g., $l_x = 150$ nm), it is possible to achieve an absorptance of 99.68% at 1550 nm with $l_y = 322.88$ nm, $l_z = 333$ nm, $\Delta d_{\mathrm{avg}} = 90$ nm, and $\Delta d = 39$ nm, and the corresponding Q factor of the absorption peak is increased to 671, as depicted in Fig. 7(b). Increasing l_x to 200 nm allows for achieving an absorptance of 99.82% at 1550 nm and an absorption Q factor of 742 with $l_y = 293.6$ nm, $l_z = 303.2$ nm, $\Delta d_{\mathrm{avg}} = 44$ nm, and $\Delta d = 30$ nm, as shown in Fig. 7(c). Throughout the fine-tuning process of the dimer unit cell parameters, we found the absorption spectra and peak absorptance are more sensitive to parameter changes when the l_x is larger. This suggests that a dimer metasurface with a smaller l_x would have a larger fabrication tolerance for realizing perfect absorption at the targeted wavelength.

4. Conclusion

In conclusion, we have demonstrated the high-Q perfect absorption enabled by degenerate critical coupling of quasi-BIC in a dual-symmetry-perturbed all-dielectric metasurface. We utilized two types of BIC resonances, namely, $\mathrm{ED_o} - \mathrm{BIC}$ protected by TS and $\mathrm{ED_i} - \mathrm{BIC}$ protected by RS in a dimer metasurface, whose Q factors could be independently controlled by perturbing the corresponding symmetries. By finely tuning the perturbation of two symmetries, we achieved matching radiative and nonradiative Q factors to fulfill the degenerate critical coupling condition, and a high-Q perfect absorption with $> 99\%$ absorptance at $\lambda_0 = 1550$ nm and > 600 Q factor is realized on a doubly-resonant Ge dimer metasurface with a thickness of $\sim 0.2\lambda_0$. We also found the dimer unit cell with a wider width (l_x) could have a narrower absorption linewidth at the designed wavelength while it was less tolerant to fabrication imperfections. Our research provides a new design route for narrowband all-dielectric perfect absorbers for novel optoelectronic devices. However, the current design is polarization-sensitive, which may not be ideal for certain applications. To overcome this limitation, exploring multisymmetry perturbations of BICs in quadrumer metasurfaces[30,31] could be a promising direction for future investigations.

Acknowledgements

This work was supported by the National Natural Science Foundation of China (Nos. 62105172 and 62005236), the Zhejiang Provincial Natural Science Foundation

(No. LQ21F050004), the Ningbo Natural Science Foundation (No. 202003N4102), and the K. C. Wong Magna Fund in Ningbo University.

References

1. A. Kodigala, T. Lepetit, Q. Gu, *et al.*, "Lasing action from photonic bound states in continuum," Nature **541**, 196 (2017).
2. L. Xu, D. A. Smirnova, R. Camacho-Morales, *et al.*, "Enhanced four-wave mixing from multi-resonant silicon dimer-hole membrane metasurfaces," New J. Phys. **24**, 035002 (2022).
3. F. Yesilkoy, E. R. Arvelo, Y. Jahani, *et al.*, "Ultrasensitive hyperspectral imaging and biodetection enabled by dielectric metasurfaces," Nat. Photonics **13**, 390 (2019).
4. A. Solanki, S. Li, H. Park, *et al.*, "Harnessing the interplay between photonic resonances and carrier extraction for narrowband germanium nanowire photodetectors spanning the visible to infrared," ACS Photonics **5**, 520 (2017).
5. A. Armin, R. D. Jansen-van Vuuren, N. Kopidakis, *et al.*, "Narrowband light detection via internal quantum efficiency manipulation of organic photodiodes," Nat. Commun. **6**, 6343 (2015).
6. A. Lochbaum, Y. Fedoryshyn, A. Dorodnyy, *et al.*, "On-chip narrowband thermal emitter for mid-IR optical gas sensing," ACS Photonics **4**, 1371 (2017).
7. N. Liu, M. Mesch, T. Weiss, *et al.*, "Infrared perfect absorber and its application as plasmonic sensor," Nano Lett. **10**, 2342 (2010).
8. L. Meng, D. Zhao, Z. Ruan, *et al.*, "Optimized grating as an ultra-narrow band absorber or plasmonic sensor," Opt. Lett. **39**, 1137 (2014).
9. K. Fan, J. Y. Suen, X. Liu, *et al.*, "All-dielectric metasurface absorbers for uncooled terahertz imaging," Optica **4**, 601 (2017).
10. T. Inoue, M. De Zoysa, T. Asano, *et al.*, "Realization of narrowband thermal emission with optical nanostructures," Optica **2**, 27 (2015).
11. K. Koshelev, Y. Tang, K. Li, *et al.*, "Nonlinear metasurfaces governed by bound states in the continuum," ACS Photonics **6**, 1639 (2019).
12. X. Ming, X. Liu, L. Sun, *et al.*, "Degenerate critical coupling in all-dielectric metasurface absorbers," Opt. Express **25**, 24658 (2017).
13. X. Wang, J. Duan, W. Chen, *et al.*, "Controlling light absorption of graphene at critical coupling through magnetic dipole quasi-bound states in the continuum resonance," Phys. Rev. B **102**, 155432 (2020).
14. L. Huang, G. Li, A. Gurarslan, *et al.*, "Atomically thin MoS_2 narrowband and broadband light superabsorbers," ACS Nano **10**, 7493 (2016).
15. D. G. Baranov, A. Krasnok, T. Shegai, *et al.*, "Coherent perfect absorbers: linear control of light with light," Nat. Rev. Mater. **2**, 17064 (2017).
16. J. R. Piper, V. Liu, and S. Fan, "Total absorption by degenerate critical coupling," Appl. Phys. Lett. **104**, 251110 (2014).
17. J. Tian, H. Luo, Q. Li, *et al.*, "Near-infrared super-absorbing all-dielectric metasurface based on single-layer germanium nanostructures," Laser Photonics Rev. **12**, 1800076 (2018).
18. H. Li, G. Wei, H. Zhou, *et al.*, "Polarization-independent near-infrared superabsorption in transition metal dichalcogenide Huygens metasurfaces by degenerate critical coupling," Phys. Rev. B **105**, 165305 (2022).
19. J. Tian, Q. Li, P. A. Belov, *et al.*, "High-*Q* all-dielectric metasurface: super and suppressed optical absorption," ACS Photonics **7**, 1436 (2020).
20. J. Yu, B. Ma, A. Ouyang, *et al.*, "Dielectric super-absorbing metasurfaces via PT symmetry breaking," Optica **8**, 1290 (2021).
21. Y. Gao, L. Xu, and X. Shen, "*Q*-factor mediated quasi-BIC resonances coupling in asymmetric dimer lattices," Opt. Express **30**, 46680 (2022).
22. Z. Xia, H. Song, M. Kim, *et al.*, "Single-crystalline germanium nanomembrane photodetectors on foreign nanocavities," Sci. Adv. **3**, e1602783 (2017).
23. E. D. Palik, *Handbook of Optical Constants of Solids* (Academic Press, 1985).
24. Y. He, G. Guo, T. Feng, *et al.*, "Toroidal dipole bound states in the continuum," Phys. Rev. B **98**, 161112 (2018).
25. Y. Gao, J. Ge, S. Sun, *et al.*, "Dark modes governed by translational-symmetry-protected bound states in the continuum in symmetric dimer lattices," Results Phys. **43**, 106078 (2022).
26. A. C. Overvig, S. Shrestha, and N. Yu, "Dimerized high contrast gratings," Nanophotonics **7**, 1157 (2018).
27. W. Wang, Y. K. Srivastava, T. C. Tan, *et al.*, "Brillouin zone folding driven bound states in the continuum," Nat. Commun. **14**, 2811 (2023).
28. S. You, M. Zhou, L. Xu, *et al.*, "Quasi-bound states in the continuum with a stable resonance wavelength in dimer dielectric metasurfaces," Nanophotonics **12**, 2051 (2023).
29. K. Koshelev, S. Lepeshov, M. Liu, *et al.*, "Asymmetric metasurfaces with high-Q resonances governed by bound states in the continuum," Phys. Rev. Lett. **121**, 193903 (2018).
30. Y. Cai, Y. Huang, K. Zhu, *et al.*, "Symmetric metasurface with dual band polarization-independent high-Q resonances governed by symmetry-protected BIC," Opt. Lett. **46**, 4049 (2021).
31. R. Masoudian Saadabad, L. Huang, and A. E. Miroshnichenko, "Polarization-independent perfect absorber enabled by quasibound states in the continuum," Phys. Rev. B **104**, 235405 (2021).